

Physics Informed Surrogate Model for Linear Elasticity

Jin HUANG^a, Zhicheng ZHU^a, Jia HAO^{a,1}, Jiaqi LI^a and Hanqing OUYANG^a
^a*School of Mechanical Engineering, Beijing Institute of Technology, Beijing, 100081, China*

Abstract. Simulation of linear elasticity problems is widely applied in mechanical and architectural engineering, and surrogate models driven by sample data have become an effective approach to perform fast simulation. However, due to the scarce and expensive data in engineering, traditional data-driven surrogate models suffer from low accuracy. This paper proposes a new Physics Informed Surrogate Model (PISM), with the objective to accelerate the numerical simulation of linear elasticity problems. The governing equations are incorporated into the training process of neural networks as effective supplement information to sample data, which improves the prediction accuracy of surrogate models in small data scenarios. A ResNet structure is introduced to further improve predicting performance of the model. Experimental results show that the prediction accuracy of PISM is significantly higher than that of pure data-driven surrogate models under small data conditions, and the solving speed reaches 8-9 times that of the finite element method.

Keywords. Linear elasticity, Physics informed deep learning, Surrogate models

1. Introduction

The simulation of linear elasticity is to obtain the behavior of elastic objects under external forces, constraints, and other external factors. It is widely used in engineering fields such as mechanics, architecture, and materials [1-3]. The common approach is using numerical methods such as finite element methods to solve the control partial differential equations. However, during product optimization design, designers often need to continuously adjust the geometric parameters, and frequent numerical calculations will cause high time costs and computational expenses, arising the emergence of surrogate model methods.

Surrogate models based on deep learning can mine the information contained in known data and construct high-fidelity models to accurately describe the input-output relationship, which has been widely applied in fields such as image recognition [4], natural language processing [5], and genomics [6]. However, the prediction accuracy of this method depends on a large amount of high-quality sample data. In the field of linear elasticity mechanics, data usually comes from expensive numerical simulations and experimental observations. Moreover, the pure data-driven approach results in models lacking interpretability, limiting the method's application and extension. Therefore,

¹ Corresponding Author, Jia HAO, Beijing Institute of Technology, No.5 Zhongguancun South Road, Hai Dian District, Beijing, China, E-mail: j.bit@bit.edu.cn

training high-precision linear elasticity surrogate models under small data conditions has become a promising direction in engineering.

In recent years, significant progress has been made in using deep learning to solve partial differential equations, providing a new approach to the aforementioned problems. Raissi et al. proposed Physics Informed Neural Networks (PINN) which embed the governing equations into deep neural networks through regularization term constructed by automatic differentiation [7], ensuring that the predicted results comply with objective physical laws without sample data. Since then, using physical informed deep learning to solve engineering problems has attracted a lot of attention. Karniadakis et al. successfully applied PINN to solving the Euler equation [8]. Beck et al. used deep learning to solve nonlinear stochastic partial differential equations and the Kolmogorov equation [9]. Similarly, PINN have also been applied to learning flow and transport in porous media [10], as well as multi-physics subsurface transport problems [11] and more.

Although PINN have been widely used in various fields, existing studies have focused on using PINN to solve particular differential equations for specific solutions., meaning that each time a different problem is encountered the neural network needs to be retrained, incurring significant computational cost. This paper proposes a Physics Informed Surrogate Model (PISM), which combines the characteristics of PINN and surrogate model that driven by both small data and physical laws. Additionally, a ResNet architecture is introduced to further enhance the predicting performance of the model.

This study addresses a more challenging problem of constructing an effective surrogate model for solving problems with geometric variations, which is applied to simulation of linear elasticity problems and significantly shortening the prediction time while ensuring satisfactory prediction accuracy. This method has the following advantages:

- 1) Effectiveness with small data. By embedding physical laws in the model, PISM significantly improves the prediction accuracy of the surrogate model in small data scenarios.
- 2) Fast simulation for geometry changes. When the geometric parameters of the simulated object change, the prediction speed of PISM is 8~9 times higher than that of the FEM, while ensuring satisfactory accuracy.

2. Methods

This section introduces the basic structure of deep neural networks and explains how the PINN architecture integrates the physical laws into the training process of neural networks. Then, the principle and architecture of PISM are presented, and finally ResNet and its application effects are introduced.

2.1. Deep Neural Networks

Deep Neural Networks (DNN) consist of input layer, hidden layer(s), and output layer. It can represent complex nonlinear mappings and extract feature information from data by learning the intrinsic rules of the sample data.

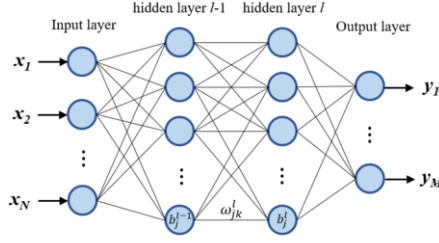


Figure 1. Deep Neural Networks

The basic framework of feedforward deep neural network is shown in Figure 1, the weights of connections between k -th neurons on hidden layer $l-1$ and j -th neurons on hidden layer l is defined as ω^l_{jk} . The input data $x_1 \dots x_N$ is propagated through the entire hidden layer to output $y_1 \dots y_M$. The deviation of j -th neurons on hidden layer l can be expressed as b^l_j . Besides, we define an activation function σ on the output of the neuron as to introduce nonlinear to the neural network. Therefore, the final output of the j -th neurons on hidden layer l is:

$$y^l_j = \sigma(a^l_j) = \sigma(\sum_k \omega^l_{jk} y^{l-1}_k + b^l_j) \tag{1}$$

A non-linear function $f(\mathbf{x}; \boldsymbol{\theta})$ is defined by a neural network, which depends on the input data \mathbf{x} and parameters $\boldsymbol{\theta} = \{\mathbf{w}; \mathbf{b}\}$. By using optimization algorithms to train the hyperparameters $\boldsymbol{\theta}$, the label data can be effectively approximated.

2.2. Physics Informed Neural Networks

The fundamental idea of physics-informed neural networks is to use automatic differentiation techniques [12] to incorporate partial differential equations into the loss function construction of neural networks, so as to approximate partial differential equations in the process of decreasing the loss function, and thereby make the training results of the neural network follow physical laws.

Consider the general form of a partial differential equation:

$$\begin{cases} N(\mathbf{u}, \lambda) = f(\mathbf{x}, t), & \mathbf{x} \in \Omega, t \in [0, T] \\ \mathbf{u}(\mathbf{x}, t) = \mathcal{B}(\mathbf{x}, t), & \mathbf{x} \in \partial\Omega, t \in [0, T] \\ \mathbf{u}(\mathbf{x}, 0) = \mathcal{I}(\mathbf{x}), & \mathbf{x} \in \Omega \end{cases} \tag{2}$$

Where \mathbf{u} is the solution of the above partial differential equation, $N(\mathbf{u}, \lambda)$ is a nonlinear operator with parameters, Ω is a subset of Euclidian space \mathbb{R}^D , T is the termination time, $\mathcal{I}(\mathbf{x})$ is the initial condition of the equation, $\mathcal{B}(\mathbf{x}, t)$ is the boundary condition of the equation.

In PINN, the inputs of network are spatial and temporal variables, i.e. \mathbf{x} and t in the Cartesian coordinate system. We define $\hat{\mathbf{u}}(\mathbf{x}, t; \boldsymbol{\theta})$ as the approximation of partial

differential equation \mathbf{u} by neural network, the Loss function of PINN can be defined by Mean Square Error (MSE):

$$Loss = Loss_{PDE} + Loss_{bc} + Loss_{ic} \quad (3)$$

Where

$$Loss_{PDE} = \frac{1}{N_r} \sum_{j=1}^{N_r} \|N(\hat{\mathbf{u}}(\mathbf{x}, t; \boldsymbol{\theta}), \lambda) - f(\mathbf{x}, t)\|^2, \quad \mathbf{x} \in \Omega, t \in [0, T] \quad (4)$$

$$Loss_{bc} = \frac{1}{N_b} \sum_{j=1}^{N_b} \|\hat{\mathbf{u}}(\mathbf{x}, t; \boldsymbol{\theta}) - \mathcal{B}(\mathbf{x}, t)\|^2, \quad \mathbf{x} \in \partial\Omega, t \in [0, T] \quad (5)$$

$$Loss_{ic} = \frac{1}{N_i} \sum_{j=1}^{N_i} \|\hat{\mathbf{u}}(\mathbf{x}, 0; \boldsymbol{\theta}) - \mathcal{I}(\mathbf{x})\|^2, \quad \mathbf{x} \in \Omega \quad (6)$$

Where $Loss_{PDE}$, $Loss_{bc}$ and $Loss_{ic}$ are the partial differential equation residuals, boundary condition residuals and initial condition residuals in the loss function respectively. N_r , N_b , $N_i \in \Omega$ are the number of sampling points corresponding to each loss function terms. Commonly used sampling methods include grid sampling method, Latin hypercube sampling, etc. The solution of the partial differential equation can be approximated by adjusting the weight parameters of neural network connections by using optimization algorithms such as gradient descent method.

2.3. Physics Informed Surrogate Model

The data-driven neural network surrogate model has been widely studied in aerodynamic design [13], topology optimization [14], etc. However, the effectiveness of this method has always relied on a large data set as premise, which is its limitation. It is the norm to lack sample data in the design process of complex products. Therefore, we propose a Physics Informed Surrogate Model (PISM) that embeds physical laws in the neural network to build surrogate model which is suitable for small data conditions. Compared with the sufficient data required by traditional surrogate model, the proposed method trains the neural network with a small amount of data and physical laws, as shown in Figure 2.

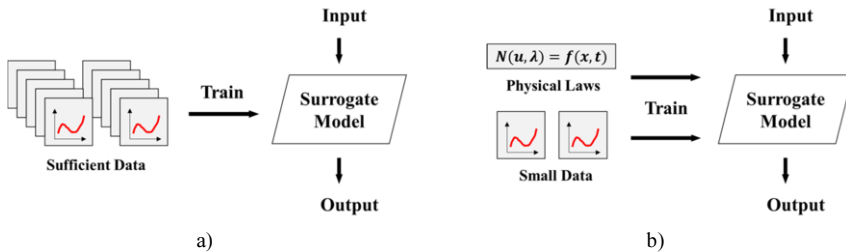


Figure 2. The difference between traditional surrogate model and physics informed surrogate model. a) traditional surrogate model; b) physics informed surrogate model

The training of PISM is shown in Figure 3. Based on the data-driven neural network, the model's output is constrained by partial differential equation constraints through automatic differentiation. During training, the neural network's output at the data point is constrained to be consistent with the sample data by the $Loss_{data}$ term in the loss function. The boundary condition term $Loss_{bc}$, initial condition term $Loss_{ic}$, and PDE term $Loss_{PDE}$ in the loss function constrain the areas where data is sparse to follow the physical laws. After the training is completed, predicting of PISM is to perform a forward propagation calculation through the neural network model saved in the training stage, no need for any neural network parameter training.

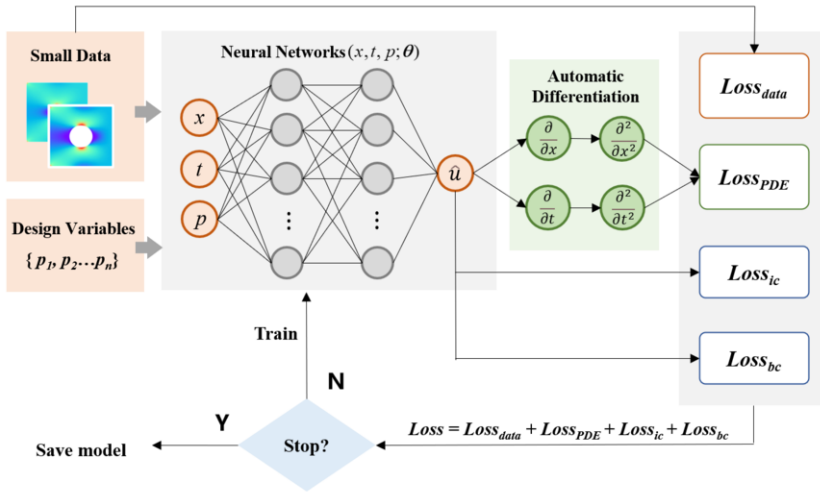


Figure 3. Training process of physics informed surrogate model.

2.4. ResNet structure

Deep neural networks extract feature information from data by adding more hidden layers. However, as the number of hidden layers increases, the network's fitting performance first increases and then decreases, a phenomenon known as degradation [15]. The reason is that neural networks find it difficult to fit the identity mapping, and therefore, the network's performance decreases after the optimal number of hidden layers is exceeded. Residual networks, or ResNet, are neural networks that incorporate skip connections to ensure the network's ability to learn identity mappings and facilitate information flow in both forward and backward directions. ResNet effectively addresses the problems of gradient vanishing and degradation, and have been widely applied in various research fields [16-17].

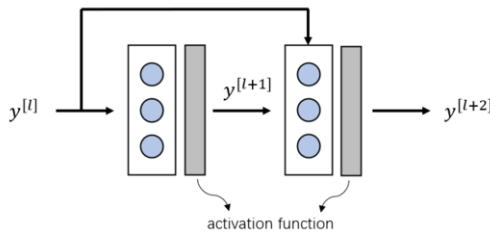


Figure 4. ResNet structure.

The structure of the ResNet is shown in Figure 4. Consider a deep neural network with two hidden layers, where $y^{[l]}$ is the output of layer l , W is the weight of the layer, and b is the bias of the layer, σ representing the activation function. Then the output of layer $l+2$ can be derived as:

$$\begin{aligned} a^{[l+1]} &= W^{[l+1]}y^{[l]} + b^{[l+1]} \\ y^{[l+1]} &= \sigma(a^{[l+1]}) \\ a^{[l+2]} &= W^{[l+2]}y^{[l+1]} + b^{[l+2]} \\ y^{[l+2]} &= \sigma(a^{[l+2]}) \end{aligned} \quad (7)$$

Residual networks introduce skip connections on top of the computation process described above. After the input vector has been processed by layer $l+1$, it is added to itself and then fed into the activation function of layer $l+2$, thus creating an identity mapping in the neural network. This is represented by:

$$y^{[l+2]} = \sigma(a^{[l+2]} + y^{[l]}) \quad (8)$$

Table 1 presents the numerical values of the loss function that the two kinds of networks converged to when used for surrogate modeling of two-dimensional linear elasticity cases. The case setting will be detailed in Section 3. The hyperparameters of both networks were set the same, and 10 experiments were conducted for each network, with the average value taken. From the table, it can be observed that using residual networks resulted in a reduction of about 18% in the training error, indicating that the application of residual networks in this study can significantly improve the predictive accuracy of the model.

Table 1. Prediction accuracy comparison between ResNet and deep neural network

	ResNet	DNN
Loss	0.002070	0.002524

3. Experiment

This section demonstrates the experimental results of applying PISM to problems in 1.1. linear elasticity. The governing equations of the problem were introduced, followed by a description of the experimental setup. Defected plate with an inner hole, a classic example for observing stress concentration issues in linear elasticity, was used for the experiment. Finally, the results were analyzed and quantified.

3.1. Linear elasticity

Consider a small deformation of a two-dimensional elastic object that is homogeneous and isotropic. The governing equations of linear elasticity are as follows:

$$\nabla \cdot \boldsymbol{\sigma} + \mathbf{F} = 0 \quad (9)$$

$$\boldsymbol{\varepsilon} = \frac{1}{2} [\nabla \mathbf{u} + (\nabla \mathbf{u})^T] \quad (10)$$

$$\boldsymbol{\sigma} = \mathbf{C} : \boldsymbol{\varepsilon} \quad (11)$$

Within the scope of statics, the external loads and constraints on the object do not vary with time, so it is only subject to boundary conditions and not initial conditions. The boundary conditions of the linear elasticity partial differential equations are divided into Dirichlet boundary conditions and Neumann boundary conditions, which are expressed as follows:

$$\mathbf{u} = \mathbf{u}_0, \quad \mathbf{x} \in \partial\Omega_u \quad (12)$$

$$\boldsymbol{\sigma} \cdot \mathbf{n} = \mathbf{p}_0, \quad \mathbf{x} \in \partial\Omega_s \quad (13)$$

In the above equations, ∇ is the gradient operator, \mathbf{F} is the body force vector, $\boldsymbol{\sigma}$ is the strain tensor, \mathbf{u} and $\boldsymbol{\sigma}$ are the displacement and stress tensors, respectively, and \mathbf{C} is the constitutive tensor. \mathbf{n} is the unit normal vector on the surface, \mathbf{p}_0 is the load at the boundary, $\partial\Omega_u$ and $\partial\Omega_s$ represent Dirichlet boundary and Neumann boundary, respectively.

3.2. Experiment setup

The experimental case is two-dimensional defected plate problem, as shown in Figure 5. The plate size is 1.0m*1.0m, fixed on the left side, and subjected to a uniform load p_x along the x-axis direction at the right end, with a magnitude of 1.0MPa. The material properties of the plate are Young's modulus $E=20\text{MPa}$ and Poisson's ratio $\mu=0.3$. There is an inner hole at the center of the plate, whose geometric parameters can be adjusted as a design variable in this case. We construct a surrogate model based on the variation of geometric parameters of the circular hole to achieve fast prediction of displacement and stress under load for different geometric parameters. Experiment 1 keeps the inner hole circular, i.e., the design variable is the radius R of the circular hole; Experiment 2 has an elliptical inner hole, with the length of its major axis A as the design variable.

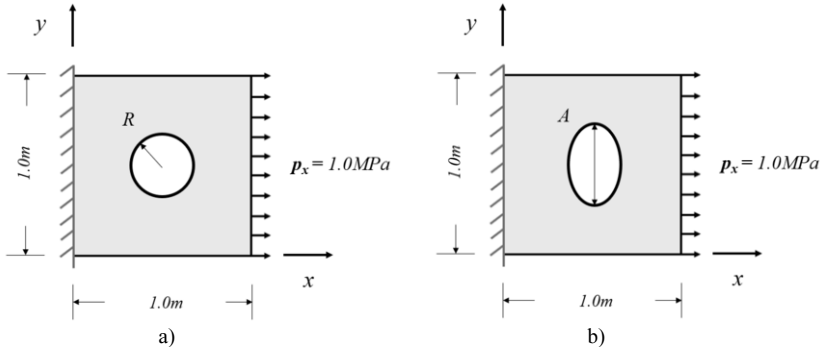


Figure 5. Experiment setup. a) Experiment 1: Plate with circular hole; b) Experiment 2: Plate with elliptical hole.

For Experiment 1, it is assumed that there are existing simulation data for three locations with R values of 0.1m, 0.15m, and 0.2m. For Experiment 2, it is assumed that there are existing simulation data for three locations with A values of 0.2m, 0.3m, and 0.4m, to simulate a small data scenario. All simulation data used in the experiments are obtained by ANSYS Workbench software using finite element method. Table 2 shows the training and testing datasets for this experiment.

Table 2. Training datasets and testing datasets for Experiment 1/2

	Training dataset (small data)			Testing dataset	
	$R=0.1m$	$R=0.15m$	$R=0.2m$	$R=0.12m$	$R=0.17m$
Experiment 1					
Experiment 2	$A=0.2m$	$A=0.3m$	$A=0.4m$	$A=0.24m$	$A=0.36m$

The neural network is structured with 15 hidden layers, with 80 neurons in each hidden layer, and uses tanh function as the activation function. The L-BFGS-B optimizer is used to train the neural network for 20,000 iterations, and the parameters $\{\mathcal{W}, \mathbf{b}\}$ of the neural network model are saved after reaching the maximum iteration or the loss function no longer decreases.

3.3. Results

3.3.1. Experiment 1: Plate with circular hole

The trained PISM is used to predict the displacement and stress of the plate under different radius R . Values of $R=0.12$ and $R=0.17$ are chosen to examine the prediction accuracy of the proposed method. Figures 6 and 7 respectively show the simulation results for x -direction displacement u and x -direction stress σ_x at $R=0.12$ and $R=0.17$. The finite element solutions are obtained by the ANSYS Workbench software. The training set of the purely data-driven surrogate model remains the same as the three sets of data in Table 2 to ensure the objectivity of the comparative experiment. The network structure, iteration times, activation function, and other parameter settings are consistent with PISM (all subsequent experiments are kept the same).

3.3.2. Experiment 2: Plate with elliptical hole

The trained PISM is used to predict the displacement and stress of the elliptical hole plate under different major axis lengths A . Figures 8 and 9 respectively show the simulation results for x -direction displacement u and x -direction stress σ_x at $A=0.24$ and $A=0.36$.

3.4. Analysis of results

Figure 10 shows the curve of the loss function with respect to the number of iterations after initialization of the neural network parameters using 20 Xavier initialization methods, using Experiment 1 as an example. It can be seen that from different initial parameters, the loss function can converge after about 10,000 iterations.

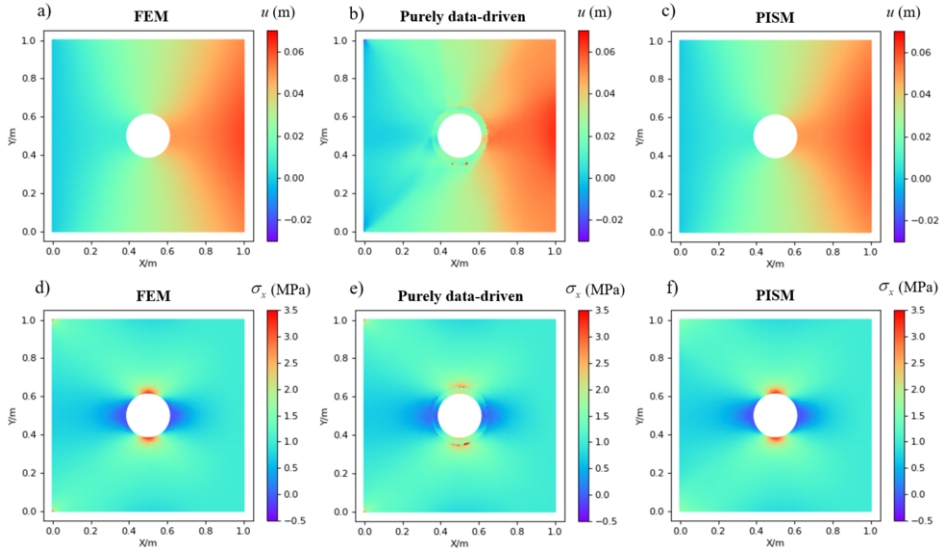


Figure 6. The prediction of u and σ_x when $R=0.12$. a) and d) are FEM solutions serving as the reference solutions; b) and e) are prediction of the purely data-driven surrogate model; c) and f) are the prediction of PISM.

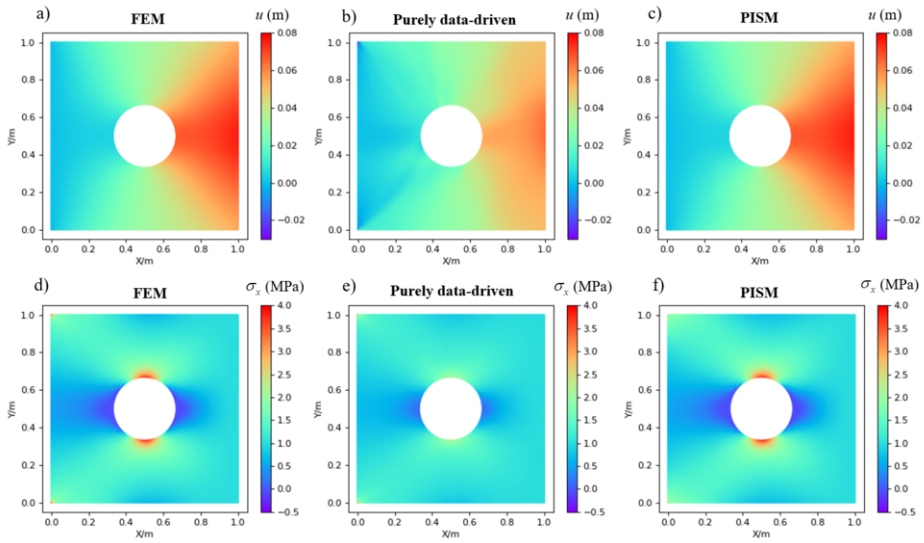


Figure 7. The prediction of u and σ_x when $R=0.17$. a) and d) are FEM solutions serving as the reference solutions; b) and e) are the prediction of purely data-driven surrogate model; c) and f) are the prediction of PISM.

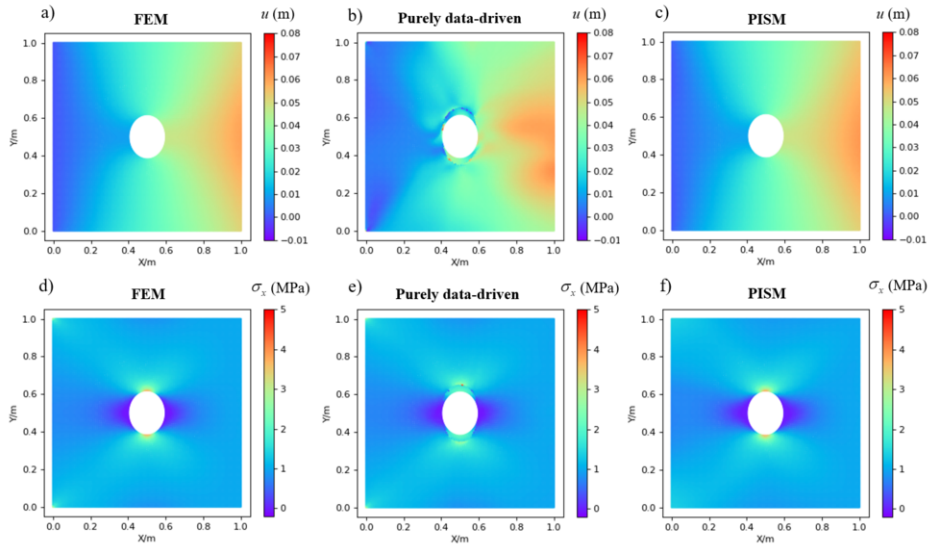


Figure 8. The prediction of u and σ_x when $A=0.24$. a) and d) are FEM solutions serving as the reference solutions; b) and e) are the prediction of purely data-driven surrogate model; c) and f) are the prediction of PISM.

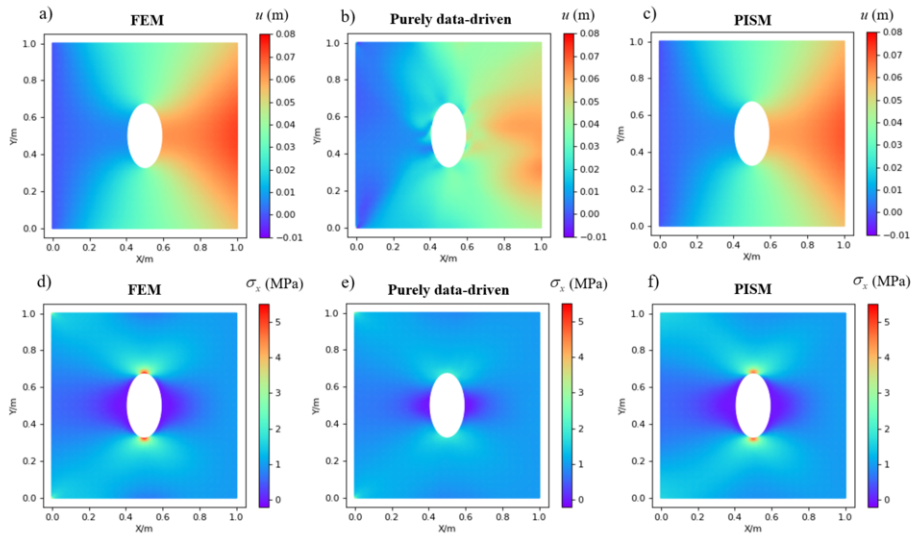


Figure 9. The prediction of u and σ_x when $A=0.36$. a) and d) are FEM solutions serving as the reference solutions; b) and e) are the prediction of purely data-driven surrogate model; c) and f) are the prediction of PISM.

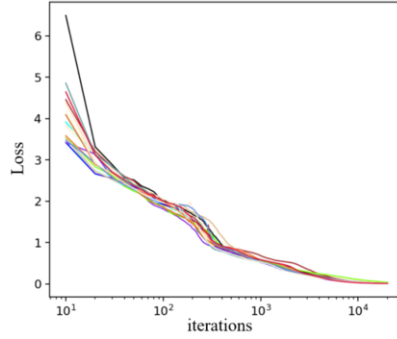


Figure 10. Curve of the loss function with respect to the number of iterations after 20 initializations.

From the observation of the experimental results shown in the above figures, it can be seen that the data-driven surrogate model cannot accurately simulate the displacement and stress fields due to the sparse data, but only predict their general trends. In contrast, the PISM can capture the details such as stress concentration more accurately, and has higher prediction accuracy. To further verify the accuracy of the proposed method, the L_2 relative error is calculated between the solutions of PISM, purely data-driven surrogate model and the finite element method. The formula for calculating the L_2 relative error is as follows:

$$\varepsilon(\mathbf{u}) = \frac{\sqrt{\sum_{i=1}^N \|\mathbf{u}(\mathbf{x}_i) - \mathbf{u}_{ref}(\mathbf{x}_i)\|^2}}{\sqrt{\sum_{i=1}^N \|\mathbf{u}_{ref}(\mathbf{x}_i)\|^2}} \quad (14)$$

where $\mathbf{u}(\mathbf{x}_i)$ is the predicted physical quantity using the surrogate model, $\mathbf{u}_{ref}(\mathbf{x}_i)$ represents the reference solution value at that point, and N is the number of coordinate points in the entire solution domain.

Table 3 and Table 4 show the L_2 errors and computational time of the two surrogate models compared to the reference solution in Experiment 1 and Experiment 2, respectively. Additionally, FEM in both experiments has 28,000~30,000 calculation nodes (varies according to geometry), and the purely data-driven surrogate model and PISM will use exactly the same points as the FEM nodes as sampling points, ensuring the fairness of the experiment. It can be seen from the tables that prediction accuracy of PISM is significantly improved compared to the purely data-driven surrogate model. At the same time, under the same computer hardware conditions (Intel Core i7-9750H CPU, RAM16GB), the prediction time of the three methods is statistically calculated, and the time consumption in the table is the average prediction time under different geometric parameters. The results show that the FEM is relatively slow because it requires a large number of numerical calculations. The computational time of the PISM and the data-driven surrogate model is very close since the two models have the same network hyperparameters, and reaching 8-9 times that of FEM.

Table 3. Experiment 1: Comparison of the relative error and prediction time consumption of the two methods

Methods	$L_2 / \%$				Time/s
	$u (R=0.12)$	$\sigma_x (R=0.12)$	$u (R=0.17)$	$\sigma_x (R=0.17)$	
FEM	-	-	-	-	1.844
purely data-driven	9.07	9.13	15.66	18.41	0.182
PISM	0.47	1.99	0.40	2.19	0.190

Table 4. Experiment 2: Comparison of the relative error and prediction time consumption of the two methods

Methods	$L_2 / \%$				Time/s
	$u (A=0.24)$	$\sigma_x (A=0.24)$	$u (A=0.36)$	$\sigma_x (A=0.36)$	
FEM	-	-	-	-	1.782
purely data-driven	10.83	8.09	16.74	21.61	0.212
PISM	4.29	3.08	2.77	3.51	0.199

4. Conclusion

This paper proposes Physics Informed Surrogate Model (PISM) for fast simulation in linear elasticity problems. PISM improves the accuracy of the surrogate model by incorporating the partial differential equation into the training process of the neural network as an effective supplement when the amount of sample data is small. A ResNet structure is introduced to alleviate the degradation problem of deep neural networks. The PISM is tested using 2D plates with circular and elliptical holes as examples and the convergence of the proposed method is verified. The results show that the accuracy of PISM predictions is significantly better than that of purely data-driven surrogate models under small data scenarios. The proposed method enables fast prediction of geometric parameter changes while ensuring high accuracy, effectively reducing the simulation time of linear elasticity. It is of significant value for fast simulation of design options in the optimization design process.

References

- [1] Georgantzinos S K, Giannopoulos G I, Anifantis N K. Numerical investigation of elastic mechanical properties of graphene structures[J]. *Materials & Design*, 2010, 31(10): 4646-4654.
- [2] Mahbod M, Asgari M. Elastic and plastic characterization of a new developed additively manufactured functionally graded porous lattice structure: Analytical and numerical models[J]. *International Journal of Mechanical Sciences*, 2019, 155: 248-266.
- [3] Sun X, Gao Z, Cao P, et al. Mechanical properties tests and multiscale numerical simulations for basalt fiber reinforced concrete[J]. *Construction and building materials*, 2019, 202: 58-72.
- [4] Krizhevsky A, Sutskever I, Hinton G E. Imagenet classification with deep convolutional neural networks[J]. *Communications of the ACM*, 2017, 60(6): 84-90.
- [5] Li H. Deep learning for natural language processing: advantages and challenges[J]. *National Science Review*, 2018, 5(1): 24-26.
- [6] Alipanahi B, Delong A, Weirauch M T, et al. Predicting the sequence specificities of DNA-and RNA-binding proteins by deep learning[J]. *Nature biotechnology*, 2015, 33(8): 831-838.

- [7] Raissi M, Perdikaris P and Karniadakis G E, Physics-informed neural networks: A deep learning framework for solving forward and inverse problems involving non-linear partial differential equations, *J. Comput. Phys.*, 378 (2019) 686-707.
- [8] Mao Z, Jagtap A D, Karniadakis G E. Physics-informed neural networks for high-speed flows[J]. *Computer Methods in Applied Mechanics and Engineering*, 2020, 360: 112789.
- [9] Beck C, Weinan E, and Jentzen A. Machine learning approximation algorithms for high-dimensional fully nonlinear partial differential equations and second-order backward stochastic differential equations[J]. *Journal of Nonlinear Science*, 2019, 29(4), 1563-1619
- [10] JIN Xiaowei, CAI Shengze, LI Hui, et al. NSFnets (NavierStokes flow nets): Physics-informed neural networks for the incompressible Navier-Stokes equations [J]. *Journal of Computational Physics*, 2021, 426: 109951.
- [11] He Q Z, Barajas-Solano D, Tartakovsky G, et al. Physics-informed neural networks for multiphysics data assimilation with application to subsurface transport[J]. *Advances in Water Resources*, 2020: 103610.
- [12] BAYDIN A G, PEARLMUTTER B A, RADUL A A, et al. Automatic differentiation in machine learning: a survey[J]. *Journal of Machine Learning Research*, 2018, 18: 1-43.
- [13] Sun G, Wang S. A review of the artificial neural network surrogate modeling in aerodynamic design[J]. *Proceedings of the Institution of Mechanical Engineers, Part G: Journal of Aerospace Engineering*, 2019, 233(16): 5863-5872.
- [14] White D A, Arrighi W J, Kudo J, et al. Multiscale topology optimization using neural network surrogate models[J]. *Computer Methods in Applied Mechanics and Engineering*, 2019, 346: 1118-1135.
- [15] He K, Zhang X, Ren S, et al. Deep residual learning for image recognition[C]//*Proceedings of the IEEE conference on computer vision and pattern recognition*. 2016: 770-778.
- [16] Wen L, Li X, Gao L. A transfer convolutional neural network for fault diagnosis based on ResNet-50[J]. *Neural Computing and Applications*, 2020, 32: 6111-6124.
- [17] Farooq M, Hafeez A. Covid-resnet: A deep learning framework for screening of covid19 from radiographs[J]. *arXiv preprint arXiv:2003.14395*, 2020.